ISSN 1062-8738, Bulletin of the Russian Academy of Sciences. Physics, 2016, Vol. 80, No. 2, pp. 149–155. © Allerton Press, Inc., 2016.
Original Russian Text © V.V. Privezentsev, V.S. Kulikauskas, V.V. Zatekin, E.P. Kirilenko, A.V. Goryachev, A.A. Batrakov, 2016, published in Izvestiya Rossiiskoi Akademii Nauk. Seriya Fizicheskaya, 2016, Vol. 80, No. 2, pp. 168–174.

Investigating $^{64}Zn^+$ Ion-Doped Silicon under Conditions of Hot Implantation

V. V. Privezentsev[a], V. S. Kulikauskas[b], V. V. Zatekin[b], E. P. Kirilenko[c], A. V. Goryachev[c], and A. A. Batrakov[d]

[a] *Institute of Physics and Technology, Russian Academy of Sciences, Moscow, 117218 Russia*
[b] *Skobeltsyn Research Institute for Nuclear Physics, Moscow State University, Moscow, 119998 Russia*
[c] *National Research University of Electronic Technology (MIET), Zelenograd, 124428 Russia*
[d] *National Research University MPEI, Moscow, 111250 Russia*
e-mail: privezentsev@ftian.ru

Abstract—The results from visualizing the structure and identifying the composition of surface and the near-surface layers of CZ n-Si (100) implanted by $^{64}Zn^+$ ions with dose of 5×10^{16} cm^{-2} and energy of 50 keV under conditions of a substrate heated to 350°C are presented. It is found that there is no Si amorphization after Zn implantation, and only one layer 200 nm thick forms and is damaged because of radiation-induced defects. Zn nanoparticles 10–100 nm in size are found on a sample's surface and in its near-surface layer. Computer analysis and mapping of the elemental and phase composition of FIB crater walls and the surface show that the main elements (54%) in the sample near-surface layer are Si, O, and Zn. The presence of ZnO phase is recorded to a depth of 20 nm in the sample.

DOI: 10.3103/S1062873816020246

INTRODUCTION

The properties of nanoparticles (NPs) of metals in different matrices have been widely investigated in recent years because they can be used in modern electronic devices [1]. Ion-implantation doping is the best way to form such NPs. Apart from purity, mobility, and so on, its main advantage is that it can be used to produce concentrations of implanted metal impurities in substrates with solubility much higher than the limiting equilibrium value. Thermal processing is used not only for annealing radiation defects, but also for the nucleation and growth of metallic NPs [2]. Investigating the implantation of metals, particularly zinc into silicon, is therefore of great importance and is now done on a large scale [3–5].

Among nanostructured materials, nanoparticles of ZnO play a special role because zinc oxide is a direct band material with a forbidden band width of 3.37 eV; it also has a high electron–hole binding energy of 60 meV in an exiton, yielding UV radiation with wavelength $\lambda = 380$ nm at temperatures of up to 450°C. Matrices with ZnO NPs can therefore be widely used in such modern optoelectronic devices as UV lasers and light-emitting diodes [6]. Their use is promising in solar cells [7], electroluminescent displays [8], gas-sensing units [9], biosensors [10], and so on. They can also be used in medicine for, e.g., delivering drugs to targeted organs [11] and the removal of diseased cells [12].

Nanoparticles of ZnO in can form in a silicon matrix via thermal processing in an oxidizing environment of silicon containing NPs of metallic Zn. The latter can be produced through the Zn ion doping of a silicon substrate. As mentioned above, the resulting zinc concentrations in silicon can be much higher than their limiting equilibrium solubility in silicon, $N_{Zn}^{lim} = 6 \times 10^{16}$ cm^{-3} [13] at a diffusion temperature of 1250°C.

This work presents results from investigating NP formation in a near-surface Si layer doped with Zn ions under conditions of hot implantation.

SPECIMENS AND EXPERIMENT TECHNIQUES

Our investigations were conducted using single-crystal *n*-type silicon wafers grown by the Czochralski technique with thicknesses of 350 μm, orientation (100), and electron concentrations of $n_0 = 5 \times 10^{15}$ cm^{-3}. The wafers were implanted using $^{64}Zn^+$ zinc ions with dose $D = 5 \times 10^{16}$ cm^{-2} and energy $E = 50$ keV under conditions where the substrate was heated to 350°C. The Zn^+ ion beam with current density $j \le 50$ nA/cm^2 was incident on the wafer surface at an angle of 7° to eliminate channeling.

The surface was visualized using an Auriga 39-52 scanning electron microscope (SEM) in a secondary electrons (SE) mode. The defect structure and distribution profiles of implanted Zn were studied by means of Rutherford backscattering spectroscopy (RBS) with

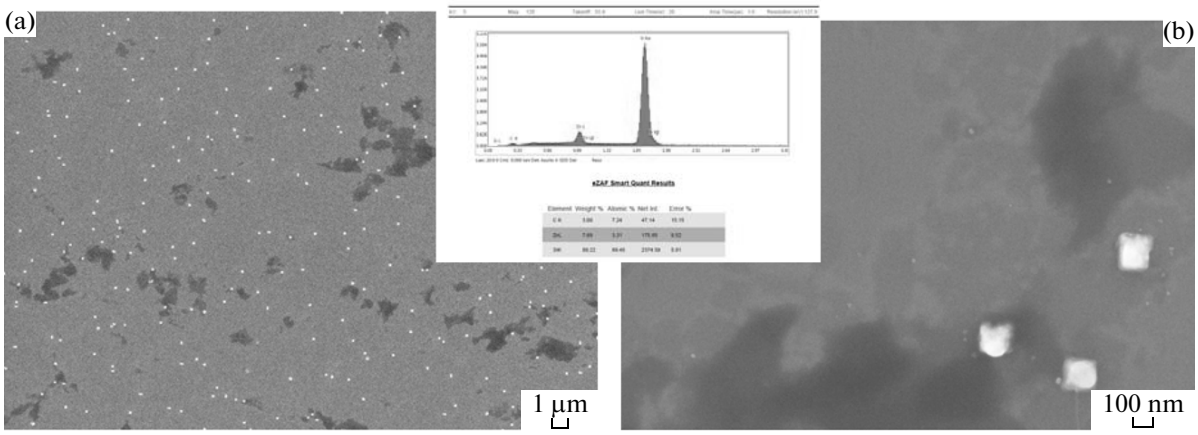

Fig. 1. SEM-SE image of the surface of the Si⟨Zn⟩ wafer at different amplifications, accompanied by the EDS spectrum of the surface (insert in the center).

He^+ ions on a Van der Graaf generator with an energy of 1.7 MeV and a scattering angle of 110° using the channeling technique. Concentration profiles of the main elements (silicon, zinc, oxygen, and the accompanying carbon) in the implanted specimens were studied via Auger-electron spectroscopy (AES) on a PHI-670 xi unit (Physical Electronics), and the etching profile was measured using an Alpha Step D-120 (KLA Tencor) device.

The complete elemental and phase compositions of the implanted layer were investigated using a SEM Versa 3D device, equippedwith a focused ion beam system (FIB) for forming the required shape of test specimens and with a unit for the energy-dispersive spectroscopy (EDS) microanalysis of elements and phases with the possibility of mapping. X-ray photoelectron spectroscopy (XPS) data with profiling over depth were investigated using a supervacuum module based on a Nanofab 50 platform (NT-MDT). The energy resolution of this spectrometer for the Au4f line was 0.9 eV. Phase composition profiles of the implanted layer were also investigated using a TOF.SIMS-5 time-of-flight secondary-ion mass spectrometer (IonTOF GmbH).

RESULTS AND DISCUSSION

Figure 1 shows the SEM-SE image of the silicon substrate's surface in two different scales: (a) coarse and (b) fine. The surface clearly exhibits NPs (white spots) with sizes of 10 to 100 nm. Judging by the observed change in contrast (more dark areas, compared to the gray background of silicon), precipitations and/or distortions of the crystalline lattice, caused by the presence of radiation-induced point defects or their clusters within the substrate at sizes of 1–10 μm, are possible. The insert in Fig. 1 shows the EDS spectrum of the specimen surface. It is evident that, in addition to the peak related to the silicon matrix (Si°*K* line, 89.45 at %), there are peaks related to the implanted zinc (Zn°*L* line, 3.31 at %) and carbon (C°*K* line, 7.24 at %). The carbon is associated with the presence of oil vapors in the vacuum system of the Auriga-39-52 electron microscope, which accumulate under the microscope electron beam (the well-known contamination phenomenon [14]).

Figure 2 shows (a) the experimental RBS spectra for the investigated specimen and (b) the model calculated profiles. Here, (*4*) is the RBS model random spectrum calculated under the same conditions. A comparison of the aligned spectra in Fig. 2a for (*1*) undoped silicon and (*3*) the zinc-implanted specimen allows us to conclude that the latter contains a great many radiation defects. This follows because of the "hump" near the boundary of the He^+ ion scattering by silicon (around channel no. 570). The damaged layer thickness was estimated at around 200 nm. A comparison of (*2*) random and (*3*) oriented RBS spectra for the implanted specimen showed that there was no silicon amorphization because spectrum (*3*) falls short of spectrum (*2*); i.e., they are not crossed.

The near-surface area of the specimen thus has only a radiation-damaged layer. The distribution profile of implanted zinc has a Gaussian shape. Based on RBS experimental spectra, we calculated the distribution profile of the Zn doping implant using the SIMNRA program [15] (see Fig. 2b, curve *2*). Its maximum was at depth $d_m = 75$ nm from the silicon wafer surface and was $N_{Zn} = 5.5 \times 10^{21}$ cm^{-3}, or 11 at %. Based on RBS experimental spectra, we also calculated the total real content of implanted Zn in the substrate (dose) using the SIMNRA program: $D_{re} = 3.4 \times 10^{16}$ cm^{-2}. The oxygen and carbon profiles were also calculated. From these it follows that the specimen surface was coated with a silicon oxide film 20 nm thick and had carbon contaminations (Fig. 2b).

Figure 3 shows the Auger-electron profiles for main elements (*3*) silicon, (*4*) implanted zinc, (*2*) oxygen, and (*1*) carbon. From Fig. 3, it follows that car-

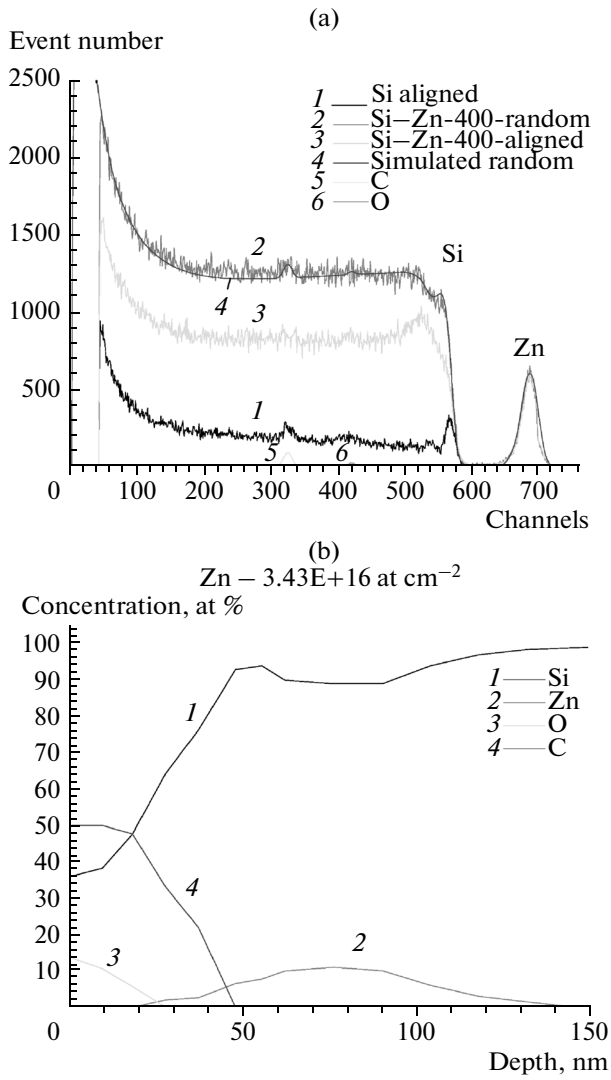

Fig. 2. (a) RBS/CT spectra and (b) Si and impurity Zn, O and C concentration profiles.

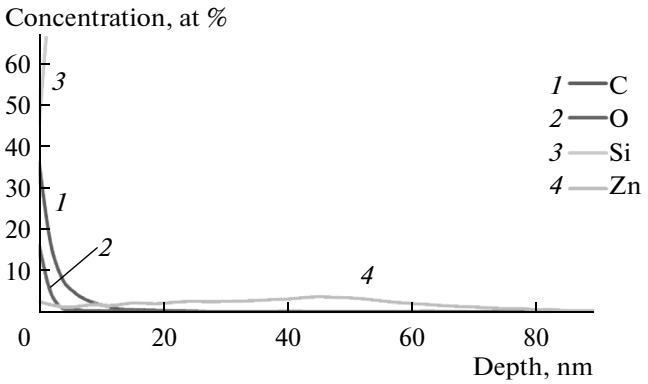

Fig. 3. Profiles of Auger-electron spectroscopy for the Si matrix, Zn and O impurities, and C contamination.

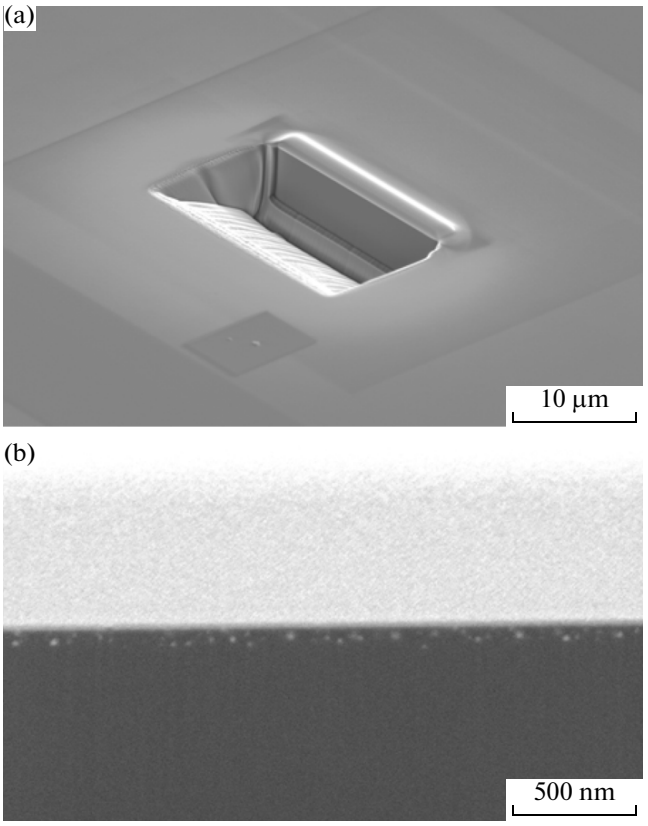

Fig. 4. SEM-SE image: (a) specimen prepared via FIB; (b) boundary between the vertical wall in the etching crater and the Si⟨Zn⟩ specimen's surface. The zinc NPs are evident against the dark background of the etching crater vertical wall near the surface.

bon contaminations at the surface were significant: 35 at %. However, they fall abruptly with depth and are already insignificant at depths of more than 15 nm. The oxygen profile indicates a surface natural film of silicon oxide SiO_2 with a thickness of about 5 nm. The profile of implanted zinc has a small burst at the surface and a main maximum of 5 at % at a depth of approximately 50 nm. The AES results generally correspond to those from RBS spectroscopy and supplement them with respect to oxygen and carbon.

Figure 4a shows an etching crater ready for analysis; Fig. 4b, the SEM-SE image of the interface of the specimen surface (above, light background) and the etching crater wall (below, dark background). Light spots are seen clearly in the upper part of the crater wall. These spots could be related to precipitates composed of elements with masses greater than those of the atoms of the silicon lattice (e.g., Zn) because emission from elements with atomic masses greater than that of the silicon matrix results a lighter background than with silicon. The size of these spots (in reality, Zn NPs) is from 10 up to 100 nm. This is supported by the EDS spectrum of the specimen's surface (see the insert in the center of Fig. 1). The spectrum has only peaks from silicon Si°*K*, implanted by Zn°*L*, and surface contamination by carbon C°*K*.

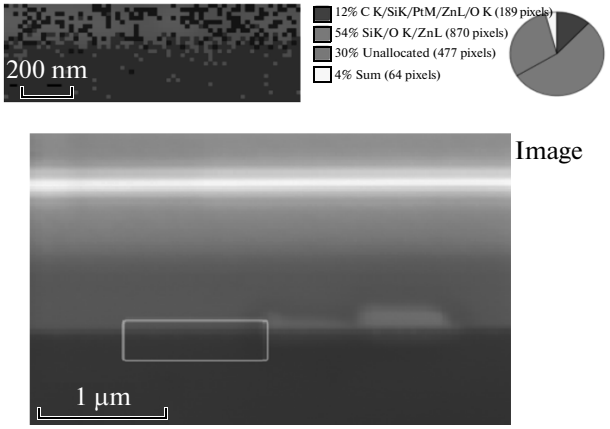

Fig. 5. Distribution map of individual phases. Superposition of phases (top left); individual phases, % : %, in tabular form (top center) and in ring diagram form (top right). SEM-SE image of the interface between the surface (light field at top) and the etching crater wall (dark field at bottom). The area investigated via EDS microanalysis is indicated by the rectangular white line.

Figure 5 shows the total EDS analysis of the composition of a selected area of the specimen (the dark lower area is the vertical wall of an etching crater in the specimen; the lighter upper area is the specimen surface). From processing the SEM-SE image shown in Fig. 5 and outlined by the white frame, using software in the set accompanying the Versa 3D unit, it follows that the preferred phase (54 at %, 870 pixels) within the implanted layer is phase (#1), composed of Si°K° 85.2 at %/C°K°7.83/O°K°3.87 at %/Zn°L° 2.4 at %/Pt°M 1.69 at %/Zn°L° 0.81 at %/Zr°L° 0.56 at %.

As is evident from the map for the distribution of different phases in Fig. 5 (shown in rectangular shape), phase (#1) is mainly distributed in the wafer depth. Next in abundance (30%, 187 pixels) is nonlocalized phase (#2) composed of C°K° 47.3 at %/Si°K°

(a)

KV: 3.5 Mag: 46126 Takeoff: 73.5 Live Time, s: 84 Amp Time, μs: 1.6 Resolution, eV: 127.9

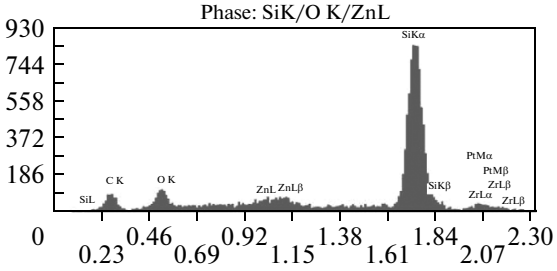

eZAF Smart Quant Results

Element	Weight, %	Atomic, %	Net Int.	Error, %
C K	3.15	7.83	5.9	16.59
O K	2.07	3.87	6.6	15.52
ZnL	1.78	0.81	2.4	27.36
SiK	80.25	85.25	86.4	11.53
ZrL	1.71	0.56	0.4	84.13
PtM	11.03	1.69	2.4	29.27

(b)

KV: 3.5 Mag: 46126 Takeoff: 73.5 Live Time, s: 46.1 Amp Time, μs: 1.6 Resolution, eV: 127.9

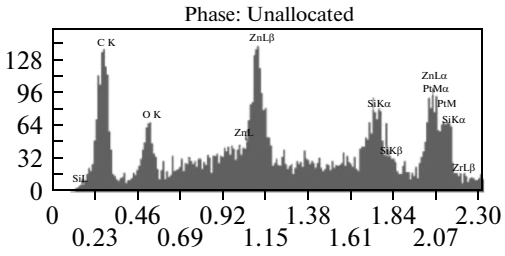

eZAF Smart Quant Results

Element	Weight, %	Atomic, %	Net Int.	Error, %
C K	10.45	47.34	17.1	14.07
O K	0.74	2.51	1.4	78.34
ZnL	1.06	0.88	0.9	73.56
SiK	14.7	28.44	11.1	20.6
ZrL	1.52	0.9	0.3	75.48
PtM	71.53	19.93	11.7	24.09

(c)

KV: 3.5 Mag: 46126 Takeoff: 73.5 Live Time, s: 84 Amp Time, μs: 1.6 Resolution, eV: 127.9

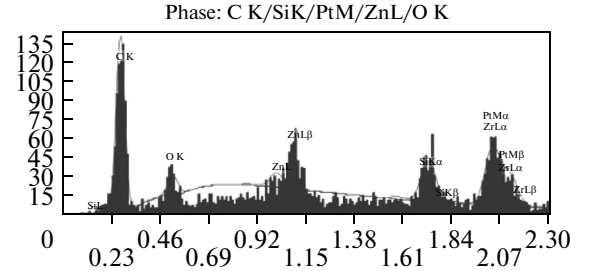

eZAF Smart Quant Results

Element	Weight, %	Atomic, %	Net Int.	Error, %
C K	13.03	51.31	35.6	14.23
O K	1.3	3.64	4.4	55.64
ZnL	2.06	1.49	3	59.55
SiK	11.7	19.71	15.5	22.24
ZrL	22.48	11.56	7.4	40.06
PtM	49.44	11.99	14.1	25.49

(d)

KV: 3.5 Mag: 46126 Takeoff: 73.5 Live Time, s: 146.4 Amp Time, μs: 1.6 Resolution, eV: 127.9

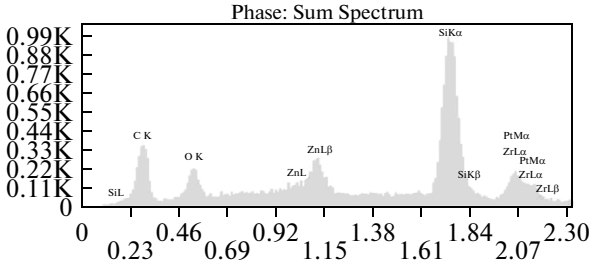

eZAF Smart Quant Results

Element	Weight, %	Atomic, %	Net Int.	Error, %
C K	6.73	20.09	13.2	12.69
O K	1.56	3.55	4.7	15.8
ZnL	1.43	0.76	1.8	30.15
SiK	52.84	67.46	54.9	11.64
ZrL	5.94	2.34	1.5	48.01
PtM	31.48	5.79	6.9	20.92

Fig. 6. EDS spectra of individual phases and corresponding tables of elements (eZAF Smart Quant Results): (a) main phase (54%, #1), (b) unseparated phase (30%, #2), (c) surface phase (12%, #3), and (d) total spectrum (4%, #4).

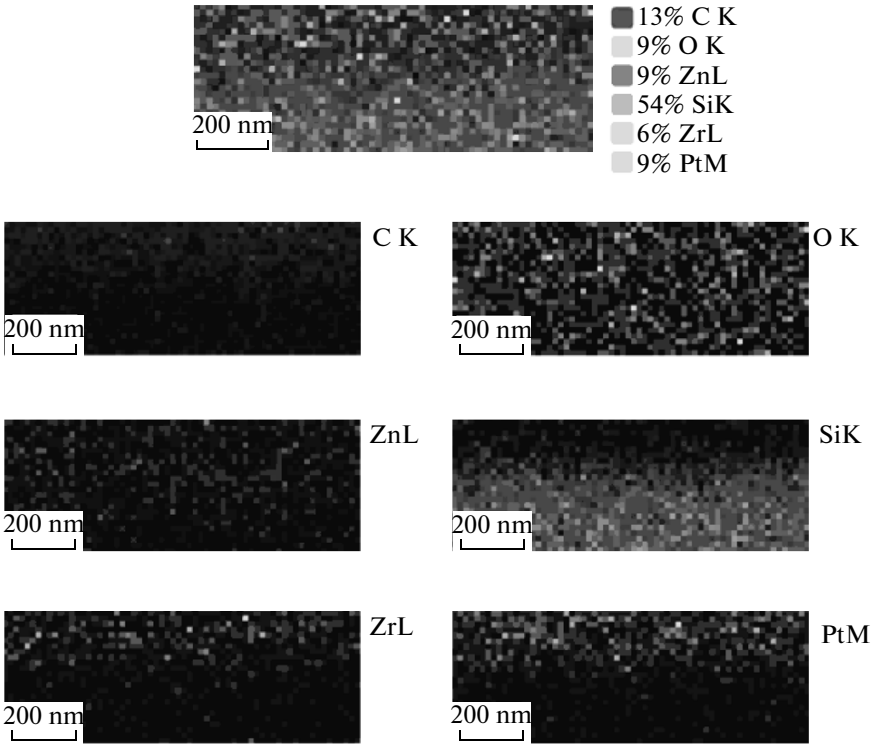

Fig. 7. Total distribution map of revealed elements in the investigated area (top center) and the distribution map of individual elements (bottom left and right).

28.4 at %/Pt°*M*° 19.9 at %/O°*K*° 1.89 at %/Zn°*L*° 0.9 at %/Zr°*L*° 0.4 at %.

It is evident that the phase (#2) is uniformly dispersed over all of the phase distribution map, due mainly to contamination of the vacuum module from working earlier with platinum Pt and zirconium Zr, and to contamination by carbon C because of the presence of oil vapors in the vacuum system of the microscope. Phase (#3) was composed of C°*K*° 51.3 at %/Si°*K*° 19.7 at %/Pt°*M*° 12.0 at %/Zr°*L*° 11.7 at %/ O°*K*° 3.84 at %/Zn°*L*° 1.49 at % (Fig. 6c). Judging from Fig. 4, this phase with carbon contamination lay on the specimen surface and can be considered a surface phase. Final total spectrum (#4) is the one least widespread (4%, 89 pixels). This spectrum is related to the overall area of investigation and represents the average value of elements in this area. In view of its relative smallness, spectrum (#4) is unnoticeable on the map. This spectrum contains elements in the ratio Si°*K*° 67.5 at %/C°*K*° 20.1 at %/Pt°*M*° 5.79 at %/O°*K*° 3.55 at %/Zr°*L*° 2.34 at %/Zn°*L*° 0.78 at %.

Figure 7 shows the total distribution map for the revealed elements (top center) and the distribution maps for individual elements in the investigated area. From these maps, it follows that contaminations of carbon C°*K* lay on the specimen surface, as might be expected. Oxygen O°*K* was uniformly distributed over the investigated area. The signal from implanted zinc Zn°*L* came from near the surface. According to computations using the SRIM program, the maximum of implanted zinc must have been at 40.5 nm for the given energy [16]; however, this program does not consider effects associated with hot implantation. Therefore, as was mentioned above, the real maximum of the zinc concentration profile lay much deeper: at a depth of 60 nm, according to our experiment. Atoms of the silicon Si°*K* matrix were mainly distributed in the specimen depth, since there was surface contamination and implanted zinc impurities near the surface. Contamination of the specimen's surface by Zirconium Zr°*L* and platinum Pt°*M* was noted above.

Figure 8 presents the TOF SIMS profiles of analyzed ions and the energy spectrum for the area corresponding to ZnO^{-} ions. Profile analysis shows that the maximum of the implanted zinc was at a depth of about 50 nm, and at the silicon specimen surface was an oxide film of $SiO \cdot SiO_2$ composition. In addition, a ZnO phase formed in the near-surface layer, and it is evident from its TOF SIMS profile that ZnO was recorded to a depth of approximately 20 nm after the implantation of zinc into silicon. This is slightly more than the thickness of silicon oxide SiO_2, which (according to different data) was up to 20 nm.

Figure 9 shows the XPS spectra of (a) zinc Zn 2*p*3/2 and (b) silicon Si 2p3/2. The slight shift of the maxi-

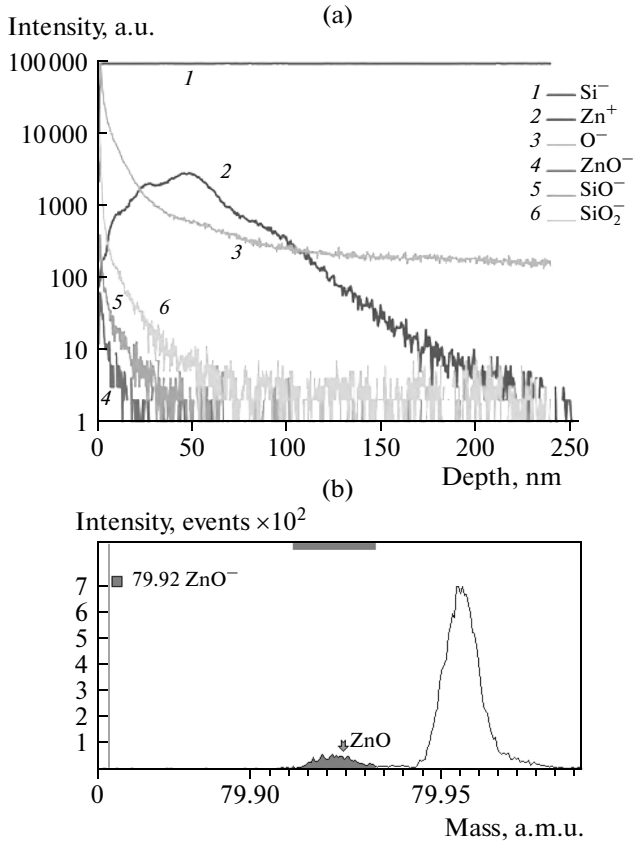

Fig. 8. (a) TOF SIMS profiles and (b) the ZnO^- ion mass spectrum.

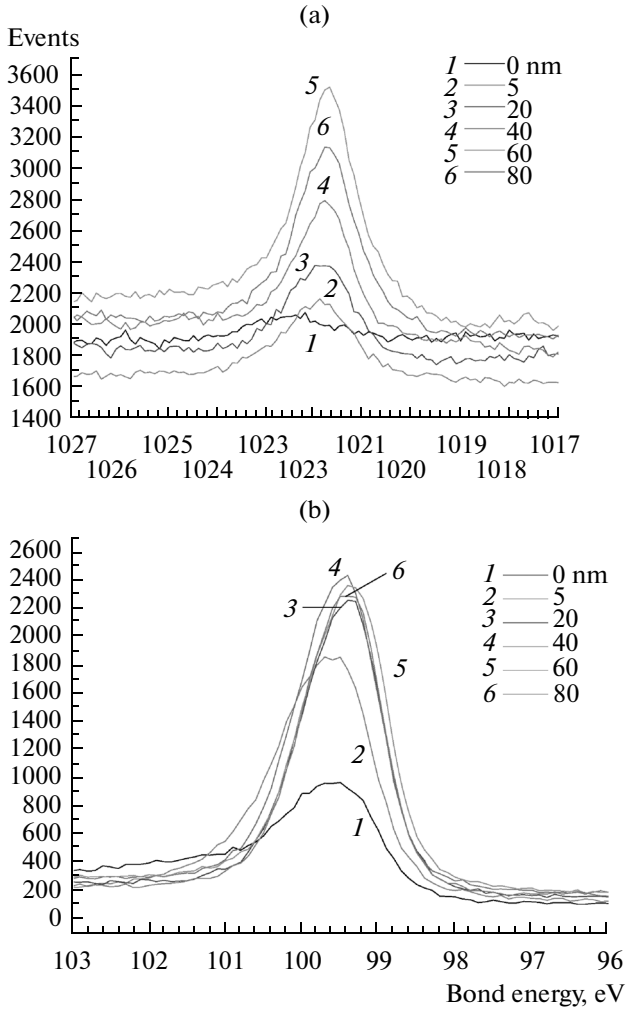

Fig. 9. XPS spectra for (a) zinc Zn 2*p*3/2 and (b) silicon Si 2*p*3/2.

mum for zinc binding energy from 1023.5 eV (curve *1*) at the surface to 1022.1 (curve *3*) at a depth of 20 nm indicates that the specimen contained the ZnO phase to a depth of 20 nm. The position of this maximum does not change at great depths; i.e., the metallic zinc phase lay deeper. The maximum intensity of this peak corresponds to a depth of 60 nm, which corresponds to the abovementioned experimental data on value R_p. Analysis of the spectra of silicon Si 2*p*3/2 (Fig. 9b) shows that at depths of 20 nm or more, the signal did not change and corresponded to the initial silicon matrix. Above this depth, the signal indicated the presence of an oxide film, which is supported by the slight shift of the position of the XPS Si 2*p*3/2 binding energy signal maximum from 100.4 eV at the surface to 100.7 eV at depths of 20 nm or more.

CONCLUSIONS

(i) No amorphizated layer formed in our Zn-implanted specimen, only a layer about 200 nm thick and damaged by radiation-induced defects.

(ii) The calculated profile of implanted Zn, determined from experimental spectra, had a Gaussian shape. Its maximum lay at depth $d_m = 75$ nm and was $N_{Zn} = 5.5 \times 10^{21}$ cm^{-3}, or 11 at %. The real complete content of implanted Zn in the substrate (the complete content in the irradiated substrate) was calculated using experimental RBS spectra: $D_{re} = 3.4 \times 10^{16}$ cm^{-2}.

(iii) Profile AES analysis of the implanted layer revealed the position of the zinc concentration maximum (50 nm), the presence of a oxide layer 5 nm thick, and indicated high carbon contamination of the specimen's surface (35 at %).

(iv) Computer analysis of the elemental and phase compositions of the EDS spectra of the specimen surface and the etching crater wall, prepared via FIB, showed that the near-surface layer of the specimen contained Zn, O, and C.

(v) Main elements (54%) in the near-surface layer were Si/O/Zn.

(vi) The ZnO phase was recorded down to a depth of 20 nm in the specimen.

ACKNOWLEDGMENTS

We thank TechnoInfo Co. for the opportunity to investigate specimens using the Auriga 39-52 and Versa 3D devices.

REFERENCES

1. *Nanoclusters and Nanocrystals,* Nalwa, H.S., Ed., Am. Sci. Publ., 2003.
2. Meldrum, A.L., Haglund, R.F., Boatner, L.A., Jr., and White, C.W., *Adv. Mater.*, 2001, vol. 13, p. 1431.
3. Muntele, A., Thevenard, P., Muntele, C., Chhay, B., and Ila, D., *Mater. Res. Symp. Proc.*, 2005, vol. 829, paper B.2.21.
4. Zollo, G., Kalitzova, M., Manno, D., and Vitali, G., *J. Phys. D: Appl. Phys.*, 2004, vol. 37, p. 2730.
5. Liu, C.L., Zhao, H., Shen, Y., Jia, G., Wang, J., and Mu, X., *Nucl. Instrum. Methods Phys. Res., Sect. B*, 2014, vol. 326, p. 23.
6. Jiang, C.Y., Sun, X.W., Lo, G.Q., Kwong, D.L., and Wang, J.X., *Appl. Phys. Lett.*, 2007, vol. 90, p. 263501.
7. Smestad, G.P. and Gratzel, M., *J. Chem. Educ.*, 1998, vol. 75, p. 752.
8. Li, C., Yang, Y., Sun, X.W., Lei, W., et al., *Nanotecnology*, 2007, vol. 18, p. 135604.
9. Chu, S., Olmedo, M., Yang, Zh., et al., *Appl. Phys. Lett.*, 2008, vol. 93, p. 181106.
10. Inbasekaran, S., Senthil, R., Ramamurthy, G., and Sastry, T.P., *Int. J. Innovative Res. Sci. Eng. Technol.*, 2014, vol. 3, p. 8601.
11. Fakhar-e-Alam, M., Rahim, S., Atif, M., et al., *Laser Phys. Lett.*, 2014, vol. 11, p. 039501.
12. Namvar, F., Rahman, H.S., Mohamad, R., et al., *Evidence-Based Complementary Altern. Med.,* 2015, vol. 2015, ID 593014.
13. Milnes, A.G., *Deep Impurities in Semiconductors*, New York: Wiley-Interscience, 1973.
14. Umanskii, Ya.S., Skakov, Yu.A., Ivanov, A.N., and Rastorguev, L.N., *Kristallografiya, rentgenografiya i elektronnaya mikroskopiya* (Crystallography, X-Ray Radiography, and Electronic Microscopy), Moscow: Metallugiya, 1982.
15. http://www.sinmra.org/
16. http://www.srim.org/

Translated by S. Ordzhonikidze